Ionics (2017) 23:3265–3271
DOI 10.1007/s11581-017-2148-0

ORIGINAL PAPER

# Fabrication and electrochemical investigation of $Li_{0.5}TiO_2$ as anode materials for lithium ion batteries

**Yan Kuang**[1] · **Yuxi Chen**[1] · **Xiaohong Xia**[1] · **Yuede He**[1] · **Li Yang**[1] · **Hongbo Liu**[1]

Received: 4 February 2017 / Revised: 8 May 2017 / Accepted: 10 May 2017 / Published online: 19 June 2017
© Springer-Verlag Berlin Heidelberg 2017

**Abstract** Hexagonal and cubic $Li_{0.5}TiO_2$ particles have been fabricated through magnesiothermic reduction of $Li_2TiO_3$ particles in a temperature range of 600 to 640 °C. The prolonged reduction time results in lattice transition from hexagonal to cubic structure of $Li_{0.5}TiO_2$. Their microstructures, valance state, chemical composition, as well as electrochemical performance as anode candidates for lithium ion batteries have been characterized and evaluated. The hexagonal $Li_{0.5}TiO_2$ exhibits better electrochemical activity compared with the cubic one. Further, the carbon-coated hexagonal $Li_{0.5}TiO_2$ displays improved electrochemical performance with initial reversible capacity of 176.6 mAh $g^{-1}$ and excellent cyclic behavior except capacity fading in the initial 10 cycles, which demonstrate a novel anode candidate for long lifetime lithium ion batteries.

**Keywords** Anode · Charging/discharging · Electrochemical characterizations · Lithium batteries

## Introduction

Lithium titanate compounds, such as spinel type $Li_4Ti_5O_{12}$ [1–8], spinel type $LiTi_2O_4$ [9–14], and ramsdellite structured $Li_2Ti_3O_7$ [15–17], have been extensively investigated as anode materials for long lifetime lithium ion batteries (LIBs), because of their excellent structural stability, electrochemical reversibility, safety, and environmental affinity. Nowadays, the $Li_4Ti_5O_{12}$-based LIBs have been commercialized and applied in electric vehicles.

To meet increasing requirements for high safety and long lifetime LIBs, searching for new-type alternative electrode materials is necessary. The ramsdellite structured lithium titanate $Li_xTiO_2$ with $x$ in a range of 0.5 to 1 has been predicted through ab initio calculations. The new phases are expected to be potential anode candidates with the lowest Li ion insertion potential among the lithium titanate family [18], which is very beneficial for enhancement of the energy density of lithium titanate-based LIBs. According to the prediction, the full lithiation of $Li_xTiO_2$ results in $LiTiO_2$ with orthorhombic *Pbnm* symmetry.

Electrochemical performances of the ramsdellite structured $Li_xTiO_2$ with different $x$ range have been investigated as anode candidates for LIBs, which exhibit very good electrochemical reversibility [10, 19–21]. The rock salt-type $LiTiO_2$ was obtained through electrochemical insertion of Li ions into solid anatase type $TiO_2$ in molten LiCl [22]. In addition, the rock salt-type $LiTiO_2$ was fabricated by microwave heating of the starting materials $Li_2TiO_3$ and TiO [23]. However, impurity phases $Li_2TiO_3$ and $Ti_2O$ still existed in the final products. Herein, we report a novel anode candidate for LIBs, i.e., the hexagonal $Li_{0.5}TiO_2$ fabricated through magnesiothermic reduction of $Li_2TiO_3$. The structural transition and electrochemical performance of the hexagonal $Li_{0.5}TiO_2$ have been evaluated.

## Experimental

The synthesis of $TiO_2$ and carbon-coated $TiO_2$/C was conducted in the following procedure reported elsewhere [14]. $Li_2CO_3$ was mixed with $TiO_2$ or $TiO_2$/C with molar ratio of

✉ Yuxi Chen
yxchen@hnu.edu.cn

[1] College of Materials Science and Engineering/Hunan Province Key Laboratory for Spray Deposition Technology and Application, Hunan University, Changsha 410082, China

Li/Ti equal to 2:1. The mixture was transferred to a tube furnace after being ground for 2 h and then heated at 650 °C for 8 h under Ar gas flow. After cooled down to ambient temperature, the products with or without carbon coating were washed with deionized water and dried overnight in vacuum.

The as-obtained products were mixed with Mg powders with molar ratio of 5:4, and then the mixture was transferred to a tube furnace and heated at desired temperature with desired time under protection of Ar gas flow. After cooled down to ambient temperature, the products were mixed with 1 M HCl and stirred for 2 h and then washed using deionized water and dried overnight in vacuum.

The microstructures and chemical compositions of the products were characterized by X-ray diffraction (XRD, D8 Advance), X-ray photoelectron spectroscopy (XPS, ESCALAB 250Xi), scanning electron microscopy (SEM, JSM6700F), and inductively coupled plasma atomic emission spectrometry (ICP-AES, SPECTRO BLUE SOP).

Electrodes were prepared by drying a slurry (a mixture of 70 wt% active materials, 10 wt% acetylene black, and 20 wt% polyvinylidene fluoride dissolved in 1-Methyl-2-pyrrolidone) at 120 °C for 12 h under vacuum. CR 2032 coin-type batteries were assembled with lithium metals as counter electrode. The diameter of the electrode film is 14 mm, and the active materials are ca. 3–4 mg. The electrolyte was composed of 1 M $LiPF_6$ dissolved in a mixture of ethylene carbonate, diethyl carbonate, and dimethyl carbonate with volume ratio of 1:1:1. Cyclic voltammetry (CV) measurements were performed in an electrochemical workstation (CHI600A) at scanning rate of 0.1 mV $s^{-1}$. Electrochemical impedance spectroscopy (EIS) measurements were performed by applying a sine wave with amplitude of 5.0 mV in a frequency range from 100 kHz to 0.01 Hz. The discharge–charge measurements were carried out on a battery cycler in a voltage range between 0.1 and 2.5 V (CT 2001A).

## Results and discussion

The synthesis of $Li_2TiO_3$ can be expressed by the following equation:

$$TiO_2 + Li_2CO_3 \rightarrow Li_2TiO_3 + CO_2\uparrow \cdot \quad (1)$$

And then, $LiTiO_2$ can be obtained through magnesiothermic reduction of the as-synthesized $Li_2TiO_3$,

$$2Li_2TiO_3 + Mg \rightarrow 2LiTiO_2 + MgO + Li_2O \quad (2)$$

MgO and $Li_2O$ can be washed out from the products using diluted HCl solution. Finally, $LiTiO_2$ is expected to be obtained.

Figure 1 exhibits XRD pattern of the products synthesized through reaction (1), which can be indexed as $Li_2TiO_3$

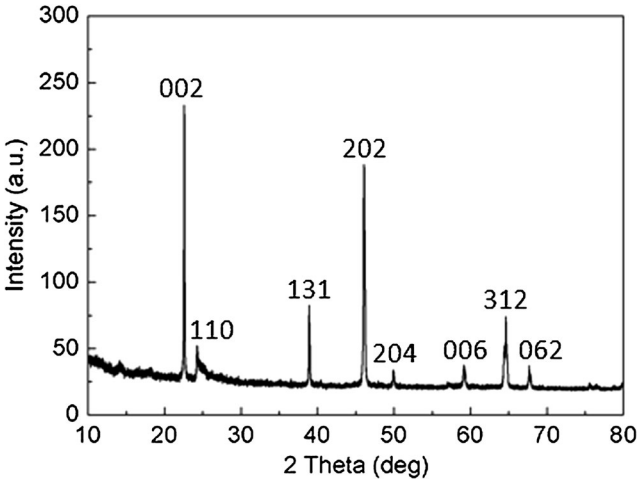


**Fig. 1** XRD pattern of the $Li_2TiO_3$ particles

(JCPDS No. 33-0831) with monoclinic structure (space group *C*2/*c*). No other phase is resolved by XRD, implying high purity of the products. The sharp reflection peaks indicate that the as-synthesized $Li_2TiO_3$ has high crystallinity. SEM image of $Li_2TiO_3$ is shown in Fig. 2, which displays secondary aggregation morphology with sizes in a range of several hundred nanometers. It also can be seen that the primary particle sizes are less than 100 nm.

Figure 3a displays XRD patterns of the products fabricated through magnesiothermic reduction (Eq. (2)) with temperature ranging from 600 to 640 °C. It can be seen that the reduction products fabricated at 600, 620, and 640 °C exhibit the same reflection positions, where reflection peaks appear at $2\theta$ = 18.7°, 43.57°, and 63.37° and corresponding to lattice spacing 0.473, 0.207, and 0.147 nm, respectively. The XRD patterns can be indexed as hexagonal $LiTiO_2$ (JCPDS No. 40-1053, $a$ = 0.2881 nm, $c$ = 1.4602 nm) through careful identification of each possible Li-Ti-O compound. The standard

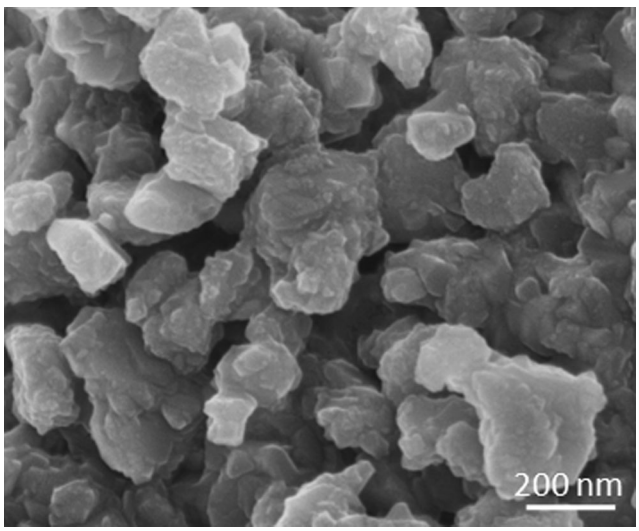


**Fig. 2** SEM image of the $Li_2TiO_3$ particles

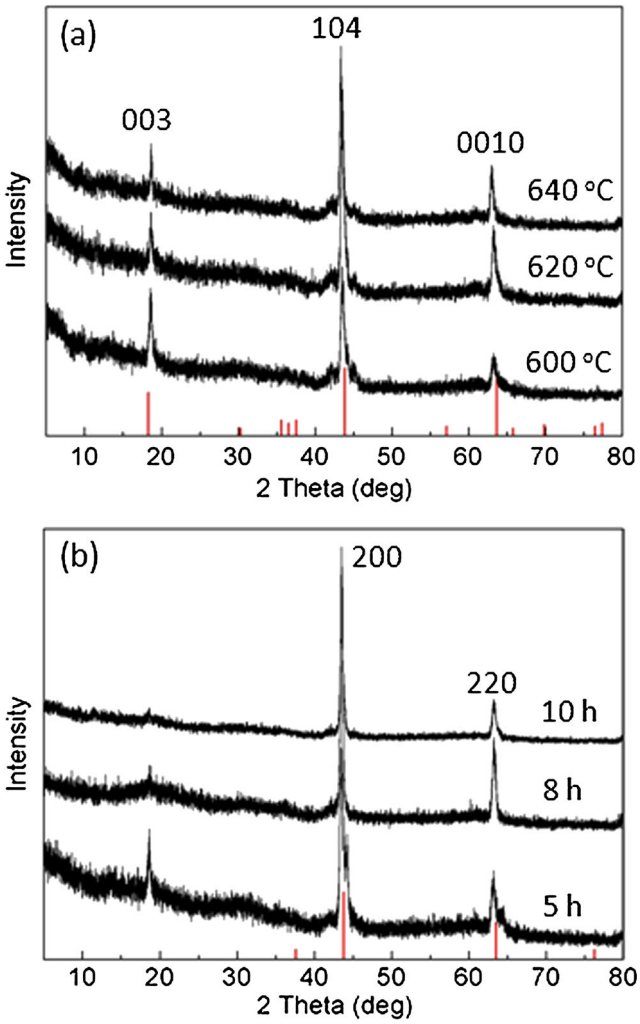


**Fig. 3** XRD patterns of the magnesiothermic reduction products **a** in a temperature range of 600 to 640 °C and **b** at 600 °C with different reduction time. The *red lines* in the bottom of **a** and **b** are the standard reflection positions of hexagonal and cubic $Li_{0.5}TiO_2$, respectively

reflection positions of the hexagonal $LiTiO_2$ are also exhibited in the bottom of the figure, where the main reflection positions {003}, {104}, and {0010} are consistent with the experimental ones. Figure 3a demonstrates that hexagonal $LiTiO_2$ can be obtained through magnesiothermic reduction (Eq. (2)) in a temperature range of 600 to 640 °C. It should be noted that additional unknown reflection peaks appear when the fabrication temperature is below 600 °C or above 640 °C, indicating formation of impurity phases (not shown).

ICP-AES measurements were performed to determine the contents of Li and Ti in the products (not shown). The results indicate that the molar ratio of Li/Ti is 0.5:1. Therefore, the magnesiothermic reduction products can be written as $Li_{0.5}TiO_2$.

Figure 3b depicts XRD patterns of the products obtained through magnesiothermic reduction at 600 °C with different reduction time. The XRD pattern obtained with reduction time 5 h is the same as Fig. 3a. However, the intensity of the {003}

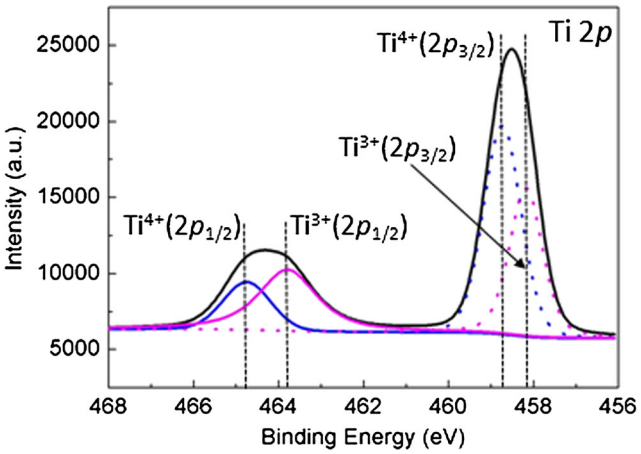


**Fig. 4** High resolution XPS spectra of Ti 2*p* peaks of the hexagonal $Li_{0.5}TiO_2$

reflection peak gradually decreases with an increase of the reduction time, and almost disappears after 10 h. Two reflection peaks remain and are located at $2\theta = 43.83°$ and 63.56°. The XRD pattern obtained through 10-h reduction can be indexed as the cubic $LiTiO_2$ (JCPDS No. 16-0223) with lattice constant $a = 0.414$ nm and space group $Fm\bar{3}m$. The standard reflection peaks of the cubic $LiTiO_2$ are displayed in the bottom of the figure. ICP–AES measurements indicate that the molar ratio of Li/Ti is the same as the hexagonal $Li_{0.5}TiO_2$. It is therefore demonstrated that hexagonal $Li_{0.5}TiO_2$ can be transited to the cubic $Li_{0.5}TiO_2$ with elongation of the reduction time.

To identify valance state of the hexagonal $Li_{0.5}TiO_2$, XPS measurements were performed. Figure 4 depicts high resolution Ti 2*p* peaks of $Li_{0.5}TiO_2$, which is composed of $Ti(2p_{3/2})$ and $Ti(2p_{1/2})$ peaks, indicating presence of $Ti^{4+}$ and $Ti^{3+}$ cations. Each of the peaks can be fitted by two peaks corresponding to $Ti^{4+}(2p_{3/2})$ (458.8 eV), $Ti^{3+}(2p_{3/2})$ (458.1 eV), $Ti^{4+}(2p_{1/2})$ (464.7 eV), and $Ti^{3+}(2p_{1/2})$ (463.7 eV), respectively. Quantitative calculations made by integration of each curve reveal that the molar content of $Ti^{3+}$ is 50% of the total titanium cations.

Subpanels a and b of Fig. 5 are SEM images exhibiting morphology of the hexagonal and the cubic $Li_{0.5}TiO_2$, respectively. It can be seen that the two products display irregular particle morphology. The particle sizes of the hexagonal $Li_{0.5}TiO_2$ are around 100 nm. However, the particle sizes of the cubic $Li_{0.5}TiO_2$ are about two times of those of the hexagonal $Li_{0.5}TiO_2$, i.e., around 200 nm. The prolonged reduction time results in particle growth.

The electrochemical performance of the products has been evaluated. Subpanels a and b of Fig. 6 are CV curves of the first three cycles of the hexagonal and the cubic $Li_{0.5}TiO_2$ with scanning rate of 0.1 mV $s^{-1}$, respectively. To compare the electrochemical performance, CV curves of the carbon-coated hexagonal $Li_{0.5}TiO_2$ is shown in Fig. 6c. Inset in

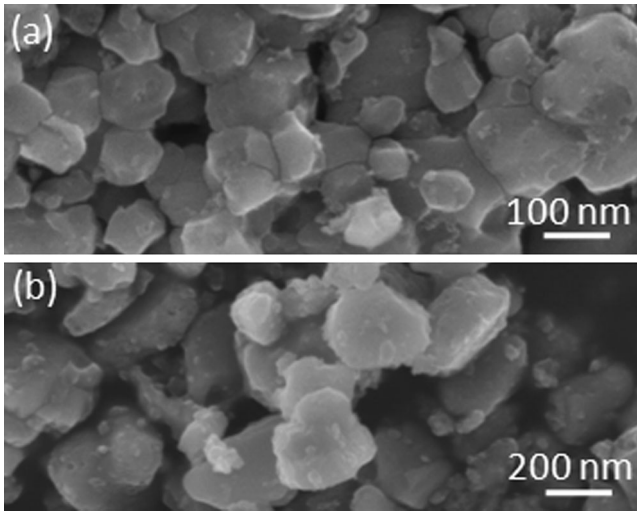


**Fig. 5** SEM images of **a** the hexagonal and **b** the cubic $Li_{0.5}TiO_2$ particles

bottom right corner is SEM image showing that the particle sizes of the carbon-coated products decrease to ca. 20 nm, which is much smaller than the uncoated $Li_{0.5}TiO_2$. The carbon content is calculated to be 8 wt% through weight loss analysis after oxidization of the carbon-coated $Li_2TiO_3$ in an open muffle furnace at 800 °C, which was further modified according to reaction (2) with target product $Li_{0.5}TiO_2$.

It can be seen that all the three products exhibit similar CV profiles. In the first CV cycle of each of the three products, two cathodic peaks appear at ca. 1.6 and 0.7 V, respectively. The cathodic peak located at ca. 1.6 V probably corresponds to the lithiation process of $Li_{0.5}TiO_2$ [18],

$$Li_{0.5}TiO_2 + 0.5Li^+ + 0.5e^- \rightleftarrows LiTiO_2. \quad (3)$$

Theoretically, the specific capacity of $Li_{0.5}TiO_2$ is calculated to be 160 mAh $g^{-1}$. Correspondingly, the anodic peaks appear at ca. 1.9, 1.9, and 1.7 V for the hexagonal, the cubic, and the carbon-coated hexagonal $Li_{0.5}TiO_2$, respectively, which represents reverse delithiation process. The decreased voltage polarization of the carbon-coated product implies high electronic and ionic conductivity. The cathodic peaks located at ca. 0.7 V are believed to be derived from formation of SEI films [24] and disappear in the subsequent cycling.

The cyclic performances of the cubic, the hexagonal, and the carbon-coated hexagonal $Li_{0.5}TiO_2$ at current density 50 mA $g^{-1}$ (ca. 0.3 C) are shown in Fig. 7a–c, respectively. In the first discharge process, all the three products exhibit much similar lithiation potential. Li ions start to insert into active materials at ca. 1.8 V, and then a long voltage slope appears, which correspond to lithiation of $Li_{0.5}TiO_2$. After that, another voltage slope appears at ca. 0.8 V, which is due to the formation of SEI films, and is consistent with CV performance. The first-cycle discharge capacities for the hexagonal, the cubic, and the carbon-coated hexagonal $Li_{0.5}TiO_2$ are

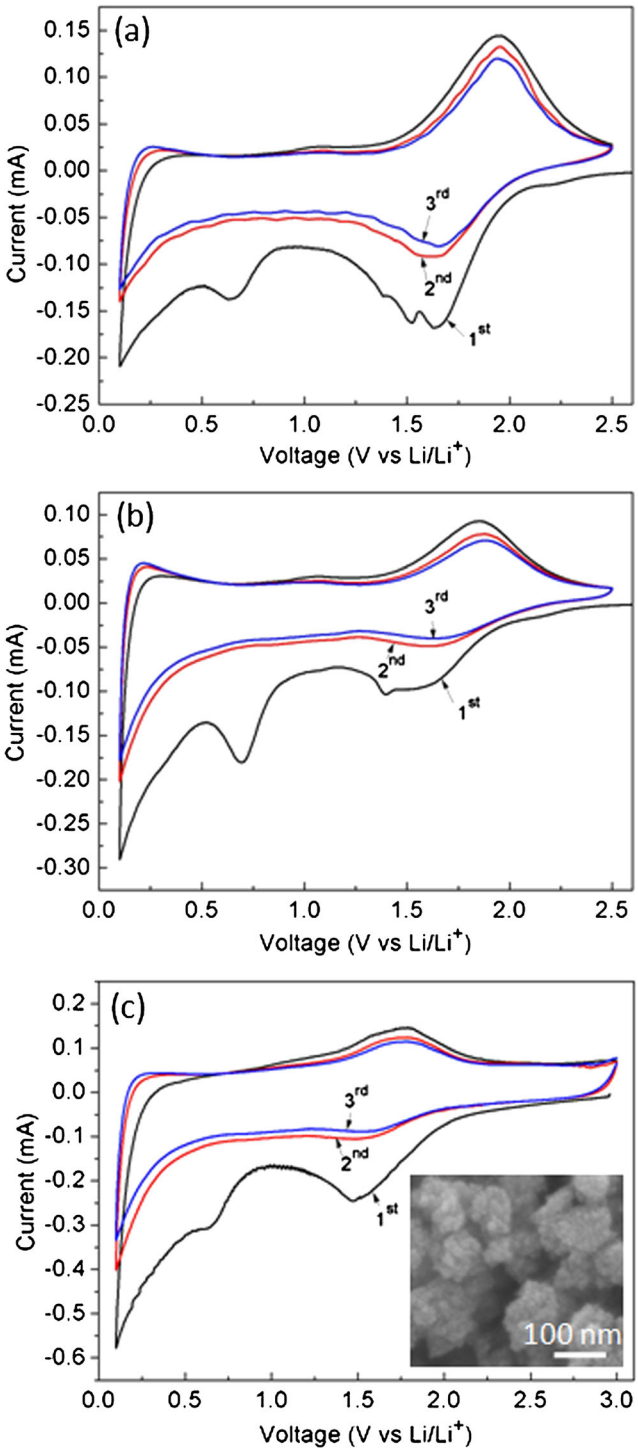


**Fig. 6** CV curves of the first three cycles of **a** the hexagonal, **b** the cubic, and **c** the carbon-coated hexagonal $Li_{0.5}TiO_2$ with a scanning rate of 0.1 mV $s^{-1}$. Inset in bottom right corner of **c** is the corresponding SEM image

277.0, 173.4, and 539.9 mAh $g^{-1}$, respectively. Correspondingly, the first-cycle charge capacities are 118.9, 68.5, and 176.6 mAh $g^{-1}$, respectively, among which the carbon-coated product delivers the highest discharge/charge capacities. The cubic $Li_{0.5}TiO_2$ exhibits the most rapid

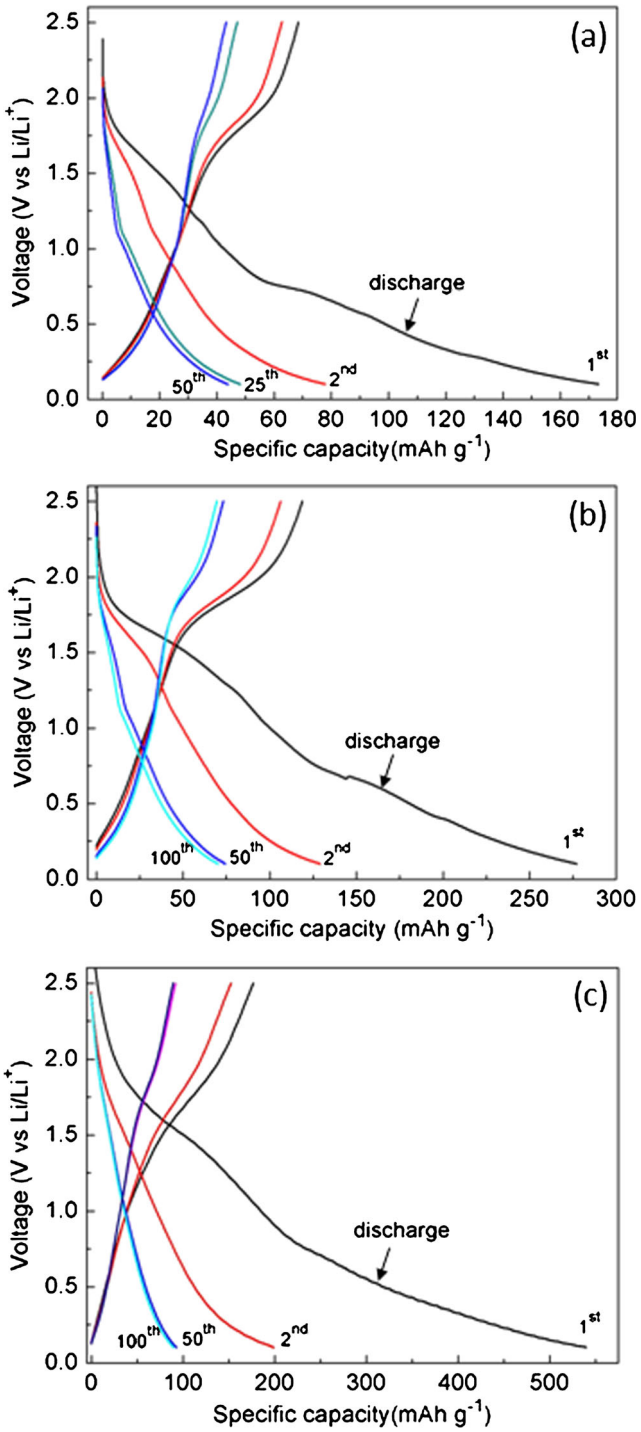


**Fig. 7** Voltage profiles of **a** the cubic, **b** the hexagonal, and **c** the carbon-coated hexagonal $Li_{0.5}TiO_2$ with current density of 50 mA $g^{-1}$

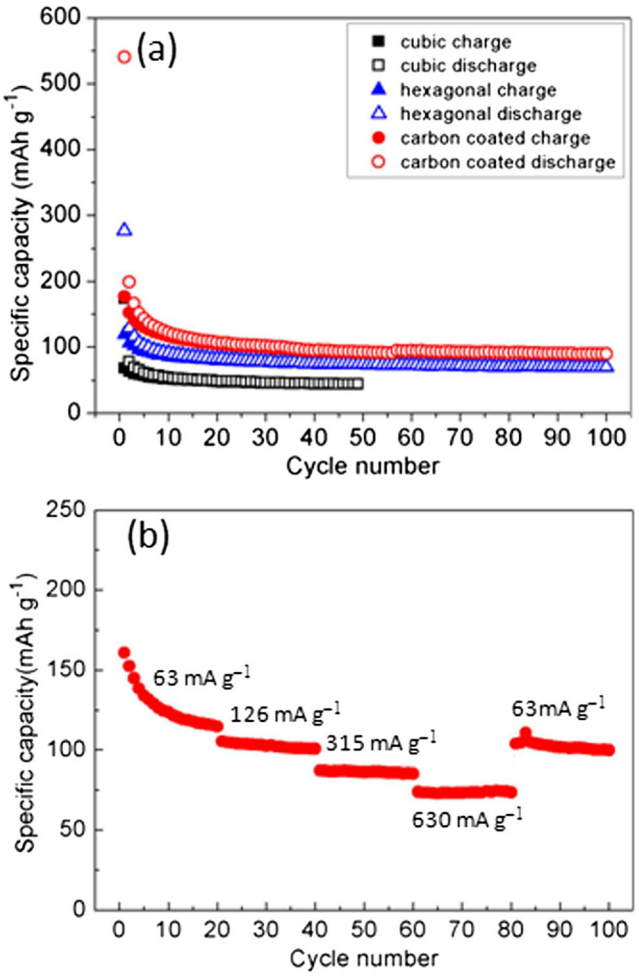


**Fig. 8** **a** Cyclic performance of the hexagonal, the cubic, and the carbon-coated hexagonal $Li_{0.5}TiO_2$ with a current density of 50 mA $g^{-1}$ and **b** rate capability of the carbon-coated hexagonal $Li_{0.5}TiO_2$

capacity fading tendency, and the discharge/charge capacities are 44.5/44.5 mAh $g^{-1}$ after 50 cycles.

The cyclic performances of the three products are shown in Fig. 8a. It can be seen that all the three products exhibit rapid capacity fading in the initial 10 cycles, and then, the capacities stabilize in the subsequent cycling. In overall, the cubic $Li_{0.5}TiO_2$ exhibits the lowest capacities, which indicates that its electrochemical activity is much limited. The electrochemical activity of the hexagonal $Li_{0.5}TiO_2$ is better than the cubic counterpart. Its reversible capacity is 69.6 mAh $g^{-1}$ after 100 cycles. The carbon coating is very effective for improvement of the electrochemical activity of the hexagonal $Li_{0.5}TiO_2$. Its first-cycle reversible capacity can reach 176.6 mAh $g^{-1}$. After 10 cycles, its reversible capacity decreases to 116.0 mAh $g^{-1}$ and then exhibits very stable cyclic performance.

The rate capability of the carbon-coated hexagonal $Li_{0.5}TiO_2$ has been evaluated, as shown in Fig. 8b. The reversible capacity fades with an increase of the current density. The initial capacity is 73.8 mAh $g^{-1}$ at current density 630 mA $g^{-1}$ (ca. 4 C), which is 60% of the 10th cycle at current density 63 mA $g^{-1}$ (123.7 mAh $g^{-1}$). The carbon-coated hexagonal $Li_{0.5}TiO_2$ delivers capacity of 103.9 mAh $g^{-1}$ when the current density recovers 63 mA $g^{-1}$ after 80 cycles at different current density. Its capacity recovery ability is 84% compared with the 10th cycle at the same current density.

To investigate electrochemical kinetics of $Li_{0.5}TiO_2$ with cycling, the hexagonal $Li_{0.5}TiO_2$ was selected and we performed EIS measurements after different discharge/charge cycling and full relaxation of the cells. The Nyquist plots of the hexagonal $Li_{0.5}TiO_2$ cells after different cycle are shown in Fig. 9a. Each of the Nyquist plots is composed of a depressed semicircle at relatively high frequency domain, followed by another depressed semicircle. A slopped line appears at low frequency domain. In order to quantitatively investigate EIS performance, an equivalent circuit was proposed to fit the Nyquist plots, as shown in Fig. 9b. The equivalent circuit consists of one solution resistance $R_s$, two units in series, each of which is composed of a resistance and a constant-phase element (CPE) in parallel, and a Warburg diffusion element $Z_w$, where the subscripts sei and ct represent SEI film and double layer charge transfer performance, respectively. It can be seen that the fitting data of each plot represented by solid curve are in good agreement with the original data. The charge transfer resistances $R_{ct}$ at different cycle are plotted as a function of cycle number (Fig. 9c). $R_{ct}$ is 148 Ω after 3 cycles and then decreases steeply to 95 Ω after 10 cycles. Then, $R_{ct}$ decreases gradually to 72 Ω after 100 cycles. Compared with the cyclic performance of the hexagonal $Li_{0.5}TiO_2$ (Fig. 8a), it can be seen that the cyclic capacity and $R_{ct}$ vary a little after 10 cycles.

The hexagonal $Li_{0.5}TiO_2$ electrodes after 100 discharge/charge cycles (full delithiation state) have been collected and washed using dimethyl carbonate, and then ex situ XRD measurements were performed to characterize the structural variation, as shown in Fig. 10. It can be seen that $Li_{0.5}TiO_2$ maintains hexagonal structure after cycling, indicating its high structural stability. The broad reflection peak located at $2\theta \approx 25°$ to 35° may be derived from the acetylene blacks in the electrode.

To date, limited investigations of $Li_{0.5}TiO_2$ have been documented. The lithiation/delithiation behavior of the hexagonal $Li_{0.5}TiO_2$ is much similar with other lithium titanate anodes [25]. However, the hexagonal $Li_{0.5}TiO_2$ displays rapid capacity fading during the initial 10 cycles. The fading mechanism is still not fully clear. The lower electrochemical performance of the cubic $Li_{0.5}TiO_2$ may be due to its larger particle size compared with the hexagonal counterpart. The enhancements of the electrochemical performance of the carbon-coated hexagonal $Li_{0.5}TiO_2$ with an initial reversible capacity of 176.6 mAh $g^{-1}$ may be ascribed to the decreased particle size and carbon coating effects compared with the uncoated counterparts, which demonstrates a novel anode candidate for long lifetime LIBs.

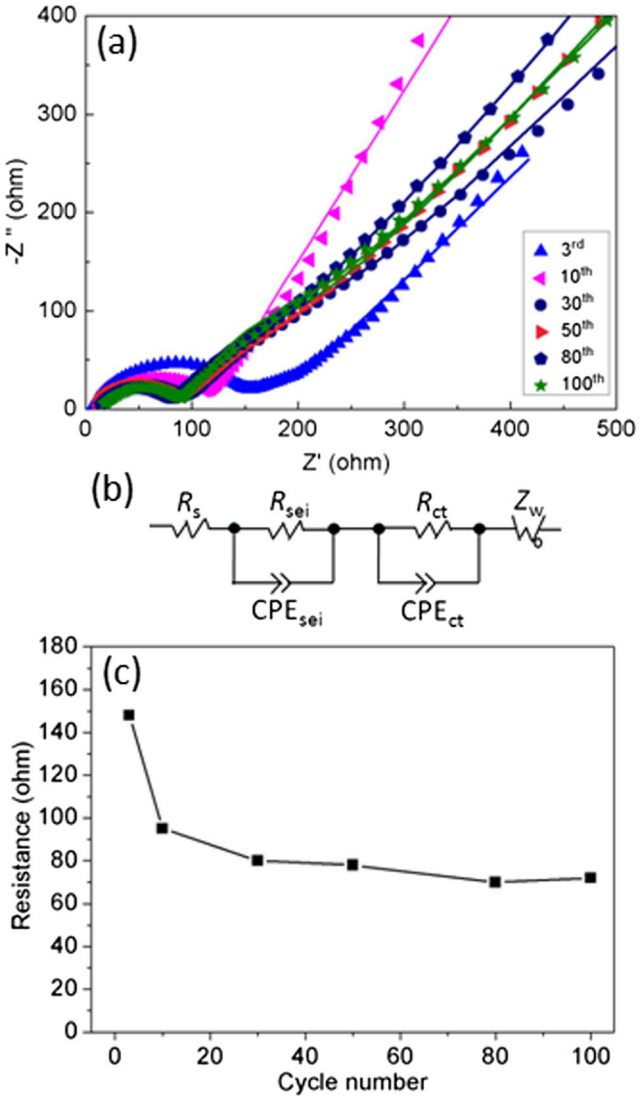


**Fig. 9** **a** Nyquist plots of the hexagonal $Li_{0.5}TiO_2$ at different cycle. *Solid curves* represent fitting data. **b** The equivalent circuit for data fitting. **c** Plot of charge transfer resistance $R_{ct}$ as a function of cycle number

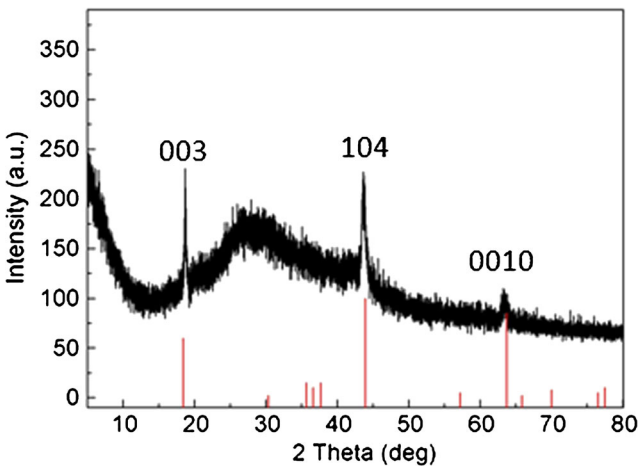


**Fig. 10** Ex situ XRD pattern of the hexagonal $Li_{0.5}TiO_2$ after 100 discharge/charge cycles. The *red lines* in the bottom are the standard reflection positions of the hexagonal $Li_{0.5}TiO_2$

## Conclusions

The hexagonal $Li_{0.5}TiO_2$ particles have been fabricated through magnesiothermic reduction of $Li_2TiO_3$ particles in a temperature range of 600 to 640 °C. The cubic $Li_{0.5}TiO_2$ particles can be obtained through prolonged reduction time. The hexagonal $Li_{0.5}TiO_2$ has high electrochemical activity compared with the cubic one as an anode candidate for LIBs. The electrochemical performance of the hexagonal $Li_{0.5}TiO_2$ has been improved after carbon coating, which delivers initial reversible capacity of 176.6 mAh $g^{-1}$ and exhibits excellent electrochemical reversibility after capacity fading in the initial 10 cycles.

**Acknowledgements** This work was supported by the National Natural Science Foundation of China (51472083 and 51402101) and Science and Technology Planning Project of Hunan Province (2016GK2064).

## References

1. Huang SH, Wen ZY, Gu ZH, Zhu XJ (2005) Preparation and cycling performance of $Al^{3+}$ and $F^-$ co-substituted compounds $Li_4Al_xTi_{5-x}F_yO_{12-y}$. Electrochim Acta 50:4057–4062
2. Ge H, Li N, Li DY, Dai CS, Wang DL (2008) Study on the effect of Li doping in spinel $Li_{4+x}Ti_{5-x}O_{12}$ ($0 \leqq x \leqq 0.2$) materials for lithium-ion batteries. Electrochem Commun 10:1031–1034
3. Li HQ, Zhou HS (2012) Enhancing the performances of Li-ion batteries by carbon-coating: presented future. Chem Commun 48: 1201–1217
4. Jung HG, Jang MW, Hassoun J, Sun YK, Scrosati B (2011) A high-rate long-life $Li_4Ti_5O_{12}/Li[Ni_{0.45}Co_{0.1}Mn_{1.45}]O_4$ lithium-ion battery. Nat Commun 2:516–520
5. Kim HK, Bak SM, Kim KB (2010) $Li_4Ti_5O_{12}$/reduced graphite oxide nano-hybrid material for high rate lithium-ion batteries. Electrochem Commun 12:1768–1771
6. Wolfenstine J, Lee U, Allen JL (2006) Electrical conductivity and rate-capability of $Li_4Ti_5O_{12}$ as a function of heat-treatment atmosphere. J Power Sources 154:287–289
7. Jung HG, Myung ST, Yoon CS, Son SB, Oh KH, Amine K, Scrosati B, Sun YK (2011) Microscale spherical carbon-coated $Li_4Ti_5O_{12}$ as ultra high power anode material for lithium batteries. Energy Environ Sci 4:1345–1351
8. Peramunage D, Abraham KM (1998) The $Li_4Ti_5O_{12}$/PAN electrolyte//$LiMn_2O_4$ rechargeable battery with passivation-free electrodes. J Electrochem Soc 145:2615–2622
9. Ra W, Nakayama M, Uchimoto Y, Wakihara M (2005) Experimental and computational study of the electronic structural changes in $LiTi_2O_4$ spinel compounds upon electrochemical Li insertion reactions. J Phys Chem B 109:1130–1134
10. Cava RJ, Murphy DW, Zahurak S, Santoro A, Roth RS (1984) The crystal structures of the lithium-inserted oxides $Li_{0.5}TiO_2$ anatase, $LiTi_2O_4$ spinel, and $Li_2Ti_2O_4$. J Solid State Chem 53:64–75
11. Kuhn A, Baehtz C, Garcia-Alvarado F (2007) Structural evolution of ramsdellite-type $Li_xTi_2O_4$ upon electrochemical lithium insertion-deinsertion ($0 \leq x \leq 2$). J Power Sources 174:421–427
12. Yang JW, Zhao J, Chen YZ (2010) Preparation and characterization of $LiTi_2O_4$ anode material synthesized by one-step solid-state reaction. Ionics 16:425–429
13. Kanno T, Awaka J, Kariya F, Ebisu S, Nagata S (2006) Electrical and magnetic properties of the spinel-type $Li(Ti_{0.8}Cr_{0.2})_2O_4$. Physica B 381:30–33
14. Pan MJ, Chen YX, Liu HB (2015) Carbon-coated spinel-structured $Li_{1-x}Ti_2O_4$ ($0<x<0.5$) anode materials with reversible two-stage lithiation potentials. Ionics 21:2417–2422
15. Garcia-Alvarado F, Arroyo de Dompablo ME, Moran E, Gutierrez MT, Kuhn A, Varez A (1999) New electrode materials for lithium rechargeable batteries. J Power Sources 81-82:85–89
16. Van Thournout M, Picard A, Womes M, Olivier-Fourcade J, Jumas JC (2006) Effect of the substitution Ti/(Fe,Ni) on the electrochemical properties of $Li_2Ti_3O_7$ as electrode materials for Li-ion accumulators. J Phys Chem Solids 67:1355–1358
17. Van Thournout M, Aldon L, Womes M, Ducourant B, Olivier-Fourcade J, Tessier C, Levasseur S (2007) Metal-doped $Li_2Ti_3O_7$ with ramsdellite structure as high voltage anode for new generation Li-ion batteries. J Power Sources 174:1270–1274
18. Koudriachova MV (2008) Ramsdellite-structured $LiTiO_2$: a new phase predicted from ab initio calculations. Chem Phys Lett 458: 108–112
19. Kuhn A, Amandi R, García-Alvarado F (2001) Electrochemical lithium insertion in $TiO_2$ with the ramsdellite structure. J Power Sources 92:221–227
20. Tsuyumoto I, Moriguchi T (2015) Synthesis and lithium insertion properties of ramsdellite $Li_xTiO_2$ anode materials. Mater Res Bull 70:748–752
21. Soares A, Fraisse B, Morato F, Ionica-Bousquet CM, Monconduit L (2012) On the synthesis conditions for tailoring lithium composition in ramsdellite phases: Application for Li-ion batteries. J Power Sources 208:440–446
22. Jiang K, Hu XH, Sun HJ, Wang DH, Jin XB, Ren YY, Chen GZ (2004) Electrochemical synthesis of $LiTiO_2$ and $LiTi_2O_4$ in molten LiCl. Chem Mater 16:4324–4329
23. Yang LH, Dong C, Guo J (2008) Hybrid microwave synthesis and characterization of the compounds in the Li–Ti–O system. J Power Sources 175:575–580
24. Goodenough JB, Kim Y (2010) Challenges for rechargeable Li batteries. Chem Mater 22:587–603
25. Zhu GN, Wang YG, Xia YY (2012) Ti-based compounds as anode materials for Li-ion batteries. Energy Environ Sci 5:6652–6667